Physics of the Earth and Planetary Interiors 266 (2017) 18–28

Contents lists available at ScienceDirect

Physics of the Earth and Planetary Interiors

journal homepage: www.elsevier.com/locate/pepi

Fully determined scaling laws for volumetrically heated convective systems, a tool for assessing habitability of exoplanets

Kenny Vilella [a,b,*], Edouard Kaminski [a]

[a] Institut de physique du globe de Paris, Sorbonne Paris Cité, CNRS, Université Paris Diderot, F-75005 Paris, France
[b] Institute of Earth Sciences, Academia Sinica, Taipei, Taiwan

ARTICLE INFO

Article history:
Received 17 January 2017
Accepted 5 February 2017

Keywords:
Internal heating
Thermal convection
Exoplanets
Thermal boundary layer
Habitability
Coreless planets

ABSTRACT

The long-term habitability of a planet rises from its ability to generate and maintain an atmosphere through partial melting and volcanism. This question has been mainly addressed in the framework of plate tectonics, which may be too specific to apply to the wide range of internal dynamics expected for exoplanets, and even to the thermal evolution of the early Earth. Here we propose a more general theoretical approach of convection to build a regime diagram giving the conditions for partial melting to occur, in planetary bodies, as a function of key parameters that can be estimated for exoplanets, their size and internal heating rate. To that aim, we introduce a refined view of the Thermal Boundary Layer (TBL) in a convective system heated from within, that focuses on the temperature and thickness of the TBL at the top of the hottest temperature profiles, along which partial melting shall first occur. This "Hottest Thermal Boundary Layer" (HotTBL) is first characterized using fully theoretical scaling laws based on the dynamics of thermal boundary layers. These laws are the first ones proposed in the literature that do not rely on empirical determinations of dimensionless constants and that apply to both low Rayleigh and high Rayleigh convective regimes. We show that the scaling laws can be successfully applied to planetary bodies by comparing their predictions to full numerical simulations of the Moon. We then use the scaling laws to build a regime diagram for exoplanets. Combined with estimates of internal heating in exoplanets, the regime diagram predicts that in the habitable zone partial melting occurs in planets younger than the Earth.

1. Introduction

In recent years the number of detected exoplanets skyrocketed (Mullally et al., 2015), thanks to the satellite Kepler (Basri et al., 2005), and of several ground based space observatories (Bakos et al., 2004; Pollacco et al., 2006). One objective of these instruments is to detect habitable planets. This requires to assess habitability based on the outputs of the detection methods, e.g., the mass and radius of a planet, and distance from its star. A key ingredient for habitability is the long-term presence of an atmosphere maintained by a continuous degassing of the planetary interior (e.g., Cockell et al., 2016; Jellinek and Jackson, 2015). Only planets where partial melting occurs can maintain an atmosphere by volcanism, which introduces a link between the internal dynamics of a planet, i.e., thermal convection, and habitability. Plate tectonics, one surface manifestation of convection within the Earth mantle, has long been recognized as a key ingredient for the evolution of life on our planet. But plate-tectonics is a specific regime and the expected variability of exoplanets internal dynamics calls for a more general approach of convection in planetary bodies.

The diagnostic of the presence of partial melting of a convective planetary mantle is based on the modeling of its thermal state which stands as a long scientific challenge, due both to the complexity of the physical problem and to the scarcity of data. For Earth, which is the best known example of convective planetary body, several questions still remain objects of debates, such as the concentration of heat producing elements in the deep mantle (McDonough and Sun, 1995; Javoy and Kaminski, 2014), the thermal state of the early Earth (Badro et al., 2015; Rubie et al., 2015) and the related existence of a primitive basal magma ocean (Labrosse et al., 2007; Andrault et al., 2011). Part of the complexity of the thermal modeling of the early Earth and subsequent thermal evolution over geological time scales, rises from the coupling between two systems with very different typical timescale that coexist in the planet, i.e., a solid mantle with a typical overturn time of ~100 Myr (McKenzie and Weiss, 1975) and a magma ocean

* Corresponding author at: Institute of Earth Sciences, Academia Sinica, Taipei, Taiwan.
E-mail address: vilella@earth.sinica.edu.tw (K. Vilella).

http://dx.doi.org/10.1016/j.pepi.2017.02.001
0031-9201/

and/or a core with a very fast dynamics (Solomatov and Stevenson, 1993; Amit et al., 2008). When considering an exoplanet the picture is even bleaker, since only its mass and radius are usually known (Spiegel et al., 2014).

One way to cope with the difficulty of handling a large number of model parameters or the coupling of systems with very different dynamics is to use analytical or semi-empirical methods such as scaling laws. As a matter of fact, scaling laws provide an interpretation of the dynamics of a whole convective system in terms of the structure and evolution of conductive boundary layers only, and as a function of a small number of dimensionless numbers that combine the different model parameters, hence making the model space much smaller. This approach was followed for example by Labrosse et al. (2001) to obtain the age of the Earth's inner core, by Ke and Solomatov (2009) to model the coupled evolution of the Martian mantle and core, and by van Hunen and Zhong (2003) to constrain the geodynamical parameters of the Hawaiian plume.

The problem of the thermal evolution of planetary mantles has been often tackled using scaling laws based on the theoretical framework of Rayleigh-Bénard convection. This formalism is indeed well suited for planets in which temperatures are kept constant at the surface and at the core mantle boundary. However, the thermal evolution of coreless rocky planets, or of differentiated planets with a small temperature difference between the core and the deep mantle, is better modeled with internal volumetrically heating only. In planetary mantles, internal heating originates from the heat released by the radioactive decay of long-lived radioactive isotopes (^{238}U, ^{235}U, ^{232}Th and ^{40}K), as well as from the secular cooling of the planet, which can be formally treated as an additional source of volumetric heating (Krishnamurti, 1968; Weinstein and Olson, 1990). Tidal heating can be a third important source of internal heating (Behounkova et al., 2011; Van Laerhoven et al., 2014) and numerical studies have shown that basal heating may also be treated as a source of internal heating (Choblet and Parmentier, 2009). Hence a purely volumetrically heated convective system provides a suitable framework to study the dynamics of planetary thermal evolution, including that of the Earth (Pollacco et al., 1993).

Scaling laws have been established for volumetrically internally heated systems by Parmentier and Sotin (2000) using numerical experiments, and by Limare et al. (2015) using lab scale experiments. However, these authors did not end with the same expression for the scaling laws, nor were able to apply them in the weak convection regime (i.e, when the system is close to the transition from conduction to convection). Furthermore, these scaling laws give a description of the Thermal Boundary Layer (TBL) that relies on an "average" thickness and an "average" temperature at its base. If such a description is useful to describe the "average" thermal state of the TBL it may not be accurate enough to determine when the system enters a regime of partial melting, because melting will occur within the hot upwellings, i.e., along the hottest vertical thermal profiles.

In this article, our aim is to propose a new set of scaling laws that characterize the thermal boundary later (temperature and thickness) above the hottest vertical thermal profiles in the fluid, that we will refer as the "Hottest Thermal Boundary Layer" or HotTBL. We will first show how the thickness and temperature of the HotTBL can be related to the convective parameters through a theoretical scaling law based on a description of the TBL at a critical stage, just before it becomes unstable and produce a cold instability. Contrary to previously published scaling laws, our expressions do not introduce any best-fitting empirical constants and are valid for any internal heating rate. We then validate the model by comparison with numerical experiments and we show how the scaling laws can be applied to planetary bodies, using the example of the Moon. Last we use the scaling laws to build a regime diagram giving the conditions for the occurrence of partial melting in planetary bodies.

2. Scaling laws for the thermal boundary layer of an internally heated fluid at infinite Prandtl number

2.1. Dimensional analysis

As a reference framework for purely internally heated convective system, we shall consider a horizontal layer of fluid with a constant temperature imposed at the top boundary and with an adiabatic condition at the base. The dynamics of the system, when it furthermore involves isoviscous and incompressible fluids, is characterized by two dimensionless numbers only, the Rayleigh number and the Prandtl number. The Rayleigh number, Ra, is defined as the ratio of the driving thermal buoyancy forces over thermal and viscous dissipation, or, equivalently, as the ratio of the rates of heat transfer by convection and heat transfer by conduction,

$$Ra = \frac{\rho g \alpha \Delta T d^3}{\kappa \eta}, \tag{1}$$

where ρ is the density, g the acceleration of gravity, α the thermal expansion coefficient, ΔT the temperature jump across the fluid layer, d the layer thickness, η the dynamic viscosity and $\kappa = \lambda/\rho C_p$ the thermal diffusivity, with λ the thermal conductivity and C_p the heat capacity. For internally heated systems, ΔT is not externally imposed but is rather related to the internal heat production,

$$\Delta T_H = H d^2/\lambda, \tag{2}$$

where H is the rate of heat generation per unit volume in the fluid. Using this temperature scale in the definition of the Rayleigh number one obtains the Rayleigh-Roberts number (Roberts, 1967),

$$Ra_H = \frac{\rho g \alpha H d^5}{\lambda \kappa \eta}. \tag{3}$$

Ra_H provides a criterion for the occurrence of convection and quantifies its vigor in internally heated fluids. Above a threshold value, called the critical Rayleigh-Roberts number ($Ra_{H,cr}$), convection appears and develops in the heated fluid. For a given Ra_H larger than $Ra_{H,cr}$, the convective interior of the fluid then consists of "active" downwellings and a rather "passive" upwelling return flow. Convection reaches a steady state spatial organization when Ra_H is slightly above $Ra_{H,cr}$, whereas the spatial organization is time dependent for larger Ra_H. The second dimensionless number, the Prandtl number (Pr), is defined as the ratio of momentum diffusivity over heat diffusivity,

$$Pr = \frac{\eta/\rho}{\kappa}. \tag{4}$$

The Prandtl number quantifies the importance of inertia relative to viscous forces, inertia being negligible for $Pr \gg 1$. In this latter case of infinite Prandtl number, convection depends only on the Rayleigh-Roberts number (Grossmann and Lohse, 2000; Grossmann and Lohse, 2001). This is the case in planetary bodies where $\eta > 10^{21}$ Pa.s and $Pr > 10^{23}$, hence in the following we will focus on the influence on Ra_H only.

As seen for example in Fig. 1 the interior of the convecting fluid consists of "active" downwellings at various stages of development (the red arrow corresponds to a fully developed downwelling and the blue arrow to the initiation of a downwelling) and a more passive return flow. The hottest thermal profile (black arrow) is found between the downwellings. One may note that the vertical change

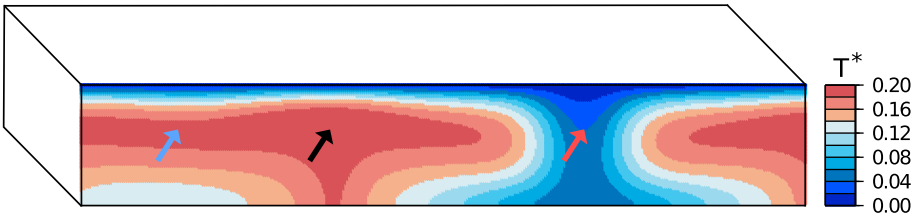

Fig. 1. A vertical slice of the dimensionless temperature field of a convective system ($T^* = T/\Delta T_H$, with ΔT_H the temperature scale defined in the text). The calculation corresponds to $Ra_H = 3.2 \times 10^4$ and free slip top and bottom boundary conditions. The growth of an instability is seen at the left side (blue arrow) and a fully developed instability is seen close to the center (red arrow). The hottest temperature profile is located between the two instabilities (black arrow). (For interpretation of the references to colour in this figure legend, the reader is referred to the web version of this article.)

of temperature along that profile mainly occurs at the top of the system, within a layer called the "Thermal Boundary Layer" (TBL). In the volumetrically heated convective system, heat is provided homogeneously in the whole layer of fluid and escapes from its surface by conduction through the TBL. The change of temperature across the TBL as well as its thickness then set the rate of heat loss of the system.

Even if the heat is transferred by conduction within the TBL, the TBL of a convective system is a dynamic structure that evolves as a function of time. Howard (1966) suggested that a TBL grows by conduction until it reaches a critical thickness at which it becomes unstable and breaks off to produce a cold instability. The spatio-temporal organization of instabilities governs in turn the dynamics of the convective system. One way to study this dynamics is then to express the temperature difference across the TBL (ΔT_{TBL}) and the thickness of the TBL (δ_{TBL}) as a function of Ra_H using dimensionless scaling laws,

$$\Delta T_{TBL}/\Delta T_H = f_{\Delta T}(Ra_H), \tag{5}$$
$$\delta_{TBL}/d = f_\delta(Ra_H), \tag{6}$$

where $f_{\Delta T}$ and f_δ are unknown functions. To determine $f_{\Delta T}$ and f_δ we follow the same line of reasoning as Jaupart and Mareschal (2011).

First we note that in the TBL heat is transferred by conduction, hence the surface heat flux ϕ scales as

$$\phi \sim \lambda \frac{\Delta T_{TBL}}{\delta_{TBL}}. \tag{7}$$

At steady state, the surface heat flux equates the heat produced in the layer of fluid, i.e., $\phi = Hd$, which yields

$$\frac{\Delta T_{TBL}}{\Delta T_H} \sim \frac{\delta_{TBL}}{d}, \tag{8}$$

hence, $f_{\Delta T} \sim f_\delta$.

To determine $f_{\Delta T}$ (or equivalently f_δ) we then consider, following Howard (1966), the dynamics of the TBL just before it becomes unstable. At that stage, the thickness of the TBL is such that there is a balance between the buoyancy force, which drives the convective flow, and the viscous drag that prevents the destabilization of the layer, i.e.,

$$\rho \alpha g \Delta T_{TBL} \sim \eta \frac{w}{\delta_{TBL}^2}, \tag{9}$$

where w is a vertical velocity scale that remains to be determined. To obtain w, we use the equation of conservation of energy in the convective system,

$$\rho C_P \frac{DT}{Dt} = \lambda \nabla^2 T + H, \tag{10}$$

where DT/Dt is the material derivative of the temperature. In the convective fluid just underneath the base of the TBL, i.e., where $T(z = d - \delta_{TBL}) = \Delta T_{TBL}$, conduction is negligible and there is a balance between vertical advection of heat and heat production, hence

$$\rho C_P \frac{w \Delta T_{TBL}}{d} \sim H, \tag{11}$$

which gives w as a function of ΔT_{TBL}. Combining Eqs. (8), (9) and (11), we finally obtain

$$\Delta T_{TBL}/\Delta T_H = C_T Ra_H^{\beta_T}, \tag{12}$$

$$\delta_{TBL}/d = C_\delta Ra_H^{\beta_\delta}, \tag{13}$$

where $\beta_T = \beta_\delta = -1/4$, whereas C_T and C_δ are (still) unknown dimensionless constants that cannot be constrained by a dimensional analysis.

2.2. A refined theory: the "critical" thermal boundary layer

The determination of the dimensionless constants C_T and C_δ has been so far empirical only. To provide theoretical constraints on C_T and C_δ, here we propose to characterize the TBL (ΔT_{TBL} and δ_{TBL}) at the onset of convection, because the TBL can be fully analytically described at that stage. Convection takes over conduction when Ra_H reaches a value called the critical Rayleigh number, $Ra_{H,cr}$. An analytic stability analysis yields $Ra_{H,cr} = 868$ for free slip mechanical boundary conditions at top and bottom (Chandrasekhar, 1961) and $Ra_{H,cr} = 2772$ for rigid boundary conditions (Roberts, 1967). Just at the onset of convection the temperature profile is still the conductive profile and the temperature reaches a maximum of $0.5\Delta T_H$ at the bottom of the system (Fig. 2). Furthermore, at this stage the TBL is simply the whole layer of fluid and verifies

$$\Delta T_{TBL} = 0.5\,\Delta T_H, \tag{14}$$
$$\delta_{TBL} = d. \tag{15}$$

Because convection occurs as soon as the critical Rayleigh-Roberts number is reached, the TBL at the onset of convection shall already follow the theoretical law obtained from the dimensional analysis of convection taking $Ra_H = Ra_{H,cr}$, even if at that stage the TBL is as thick as the whole layer of fluid. Combining the results of Eqs. (14) and (15) with the scaling laws given in Eqs. (5) and (6), we then obtain an analytical expression for C_T and C_δ,

$$C_T = 0.5\,Ra_{H,cr}^{1/4}, \tag{16}$$
$$C_\delta = Ra_{H,cr}^{1/4}. \tag{17}$$

Using these theoretical expressions, the scaling laws for the TBL can then be written as

$$\Delta T_{TBL}/\Delta T_H = 0.5\,(Ra_{H,cr}/Ra_H)^{1/4}, \tag{18}$$
$$\delta_{TBL}/d = (Ra_{H,cr}/Ra_H)^{1/4}. \tag{19}$$

These expressions, that do not rely on empirical parameters anymore, furthermore provide a physical interpretation for C_T and C_δ. Since they are functions of $Ra_{H,cr}$ only, their dependence on the boundary conditions found in previous studies

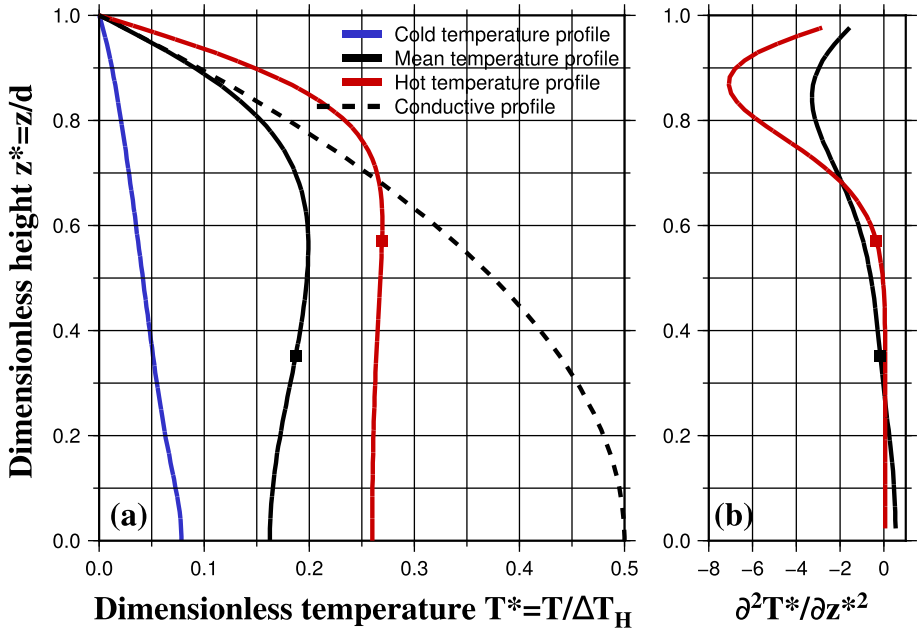

Fig. 2. Temperature profiles obtained at $Ra_H = 10^4$ and for free slip top and bottom boundary conditions. The thermal structure has reached a steady state, because the value of the Rayleigh number is close to the critical Rayleigh number. (a), The black line gives the horizontally averaged temperature profile, and the blue and red lines correspond to the coldest and hottest temperature at a given depth ("cold" and "hot" temperature profiles), respectively. The mean and hot temperature profiles show that large temperature variations only occur in the top thermal boundary layer. The black dashed line represents the conductive temperature profile which is also the temperature profile at the onset of convection. (b), Evolution of the dimensionless second derivative of the average temperature (black) and the hot temperature (red) as a function of the dimensionless height. The two squares mark the base of the thermal boundary layer defined as the first point from the top boundary where the second derivative becomes zero. The hot temperature profile yields a significantly thinner and slightly hotter thermal boundary layer than the averaged temperature profile. (For interpretation of the references to colour in this figure legend, the reader is referred to the web version of this article.)

(e.g, Choblet and Parmentier, 2009), and never explained until now to our knowledge, simply reflects the dependence of $Ra_{H,cr}$ on the boundary conditions.

The approach developed above considers the TBL at a "critical" stage, i.e., just before it becomes unstable and produce a cold instability. Previous studies (Parmentier and Sotin, 2000; Deschamps et al., 2012; Limare et al., 2015) rather consider the characteristics of an "average" TBL defined from the average thermal state of the fluid. For example, the base of the TBL can be taken as the depth at which the vertical conductive profile of the horizontally averaged temperature reaches the average internal temperature of the convective fluid (e.g., Parmentier and Sotin, 2000, hereafter referred as PS2000). In the next session we discuss the difference between our scaling laws and the ones corresponding to an "average" description of the TBL, based on their respective ability to reproduce the results of numerical simulations.

3. A numerical investigation of the "critical thermal boundary layer theory

3.1. Numerical model

We performed original numerical experiments using the code Stag3D developed by Paul Tackley, and described in detail in Tackley et al. (1994). Its application to volumetrically heated fluid is presented in Limare et al. (2015) and we provide here only a brief description of the code. Stag3D uses a finite difference multigrid technique to solve the equations of conservation of mass, momentum and energy. We consider a fluid under the Boussinesq approximation, with an infinite Prandtl number and constant properties (except density that depends on temperature). For this study, the chosen setting is a fluid purely internally heated, in a 3D Cartesian box with constant temperature at the surface and an adiabatic condition at the base. The side boundaries are reflecting, whereas the top and bottom boundary conditions can be either rigid or free slip. The input parameter is Ra_H, that ranges between 5×10^3 and 10^9. The selected aspect ratio and the space resolution of the grid (Table 1) guarantee both the development of a large number of convective currents (with a size that does not depend on the aspect ratio), and a good resolution in the TBL (more than 6 points). For computations performed at $Ra_H < 3.2 \times 10^5$, convection is steady, and we use a constant temperature in the whole box with random perturbations as the initial condition. For larger Ra_H, convection is time dependent, and a statistical steady state is reached when both the volumetric average temperature and the surface heat flux are constant (their fluctuations are zero) when averaged over several overturn times. In such cases, we use as initial condition a temperature field obtained for a previous - and smaller - Ra_H in order to reduce the computational time. We carefully checked that the final result did not depend on the choice of the initial condition.

3.2. Comparison between theory and numerical simulations

We first consider the classical description of the TBL based on the horizontally averaged temperature profile, and we compare our calculations with the results of PS2000. To determine the TBL in the numerical simulations, we consider the point where the horizontally averaged temperature is maximum along a vertical profile. We then obtain both the thickness of the TBL, δ_{TBL}, and the temperature change across the TBL, $\Delta T_{TBL} = T(z = d - \delta_{TBL})$. The final result is given in Table 2 as the best fit of the numerical results taking $\beta_T = -1/4$ or leaving it as a free fitting parameter, and it illustrates the agreement between, our numerical calculations ($C_T = 2.426$) and those of PS2000 ($C_T = 2.414$). The decrease of ΔT_{TBL} with Ra_H shown in Fig. 3(a) is well explained by Eq. (12), down to $Ra_H \sim 10^5$. The numerical results and the predictions of the scaling law however diverge for $Ra_H < 10^5$, a conclusion

Table 1
Input parameters and outputs of the numerical simulations.

$\log_{10}(Ra_H)$	Resolution	Aspect ratio	$\log_{10}\left(\frac{\Delta T_{TBL}}{\Delta T_H}\right)$ (rigid)	$\log_{10}\left(\frac{\Delta T_{TBL}}{\Delta T_H}\right)$ (free slip)	$\log_{10}\left(\frac{\delta_{TBL}}{d}\right)$ (rigid)	$\log_{10}\left(\frac{\delta_{TBL}}{d}\right)$ (free slip)
3.7	$1024 \times 1024 \times 64$	16/16	−0.338	−0.490	−0.010	−0.223
4	$1024 \times 1024 \times 64$	16/16	−0.435	−0.572	−0.199	−0.308
4.5	$1024 \times 1024 \times 64$	16/16	−0.546	−0.684	−0.308	−0.402
4.7	$1024 \times 1024 \times 64$	16/16	−0.585	−0.719	−0.367	−0.435
5	$1024 \times 1024 \times 64$	16/16	−0.639	−0.788	−0.412	−0.538
5.15	$1024 \times 1024 \times 64$	16/16	−0.679	−0.814	−0.474	−0.557
5.34	$512 \times 512 \times 64$	6/6	−0.741	−0.882	−0.516	−0.637
5.5	$512 \times 512 \times 64$	6/6	−0.779	−0.947	−0.541	−0.632
5.83	$512 \times 512 \times 64$	6/6	−0.897	−1.030	−0.656	−0.682
6	$512 \times 512 \times 64$	6/6	−0.944	−1.074	−0.670	−0.709
6.2	$512 \times 512 \times 64$	6/6	−0.991	−1.125	−0.734	−0.787
6.5	$512 \times 512 \times 64$	6/6	−1.062	−1.209	−0.767	−0.846
6.7	$512 \times 512 \times 64$	6/6	−1.110	−1.251	−0.803	−0.873
6.8	$512 \times 512 \times 64$	6/6	−1.135	−1.275	−0.837	−0.924
6.9	$512 \times 512 \times 64$	6/6	−1.158	−1.300	−0.849	−0.951
7.15	$512 \times 512 \times 64$	6/6	−1.217	−1.363	−0.931	−1.044
8	$384 \times 384 \times 128$	6/6	−1.415	−1.578	−1.162	−1.311
8.5	$384 \times 384 \times 128$	6/6	−1.533	−1.691	−1.325	−1.320
9	$512 \times 512 \times 256$	4/4	−1.663	−1.831	−1.451	−1.591

Parameters are listed for symmetrical rigid and free slip boundary conditions. The temperature difference across the thermal boundary layer (ΔT_{TBL}) and its thickness (δ_{TBL}) are made dimensionless using ΔT_H and d (see text).

Table 2
Parameters of the scaling laws of the Thermal Boundary Layer (TBL).

	C_T	β_T	C_δ	β_δ
Free slip, free exponent	2.467	−0.251	2.299	−0.168
Free slip, fixed exponent	2.426	−0.25	NA*	NA*
Rigid, free exponent	3.094	−0.244	2.129	−0.151
Rigid, fixed exponent	3.388	−0.25	NA*	NA*

To determine the parameters, the base of the TBL is set as the point where the horizontally averaged temperature profile reaches a maximum.
* The best fit exponent is too far from the theoretical −1/4 value to provide relevant results.

reached also by Deschamps et al. (2012) for calculations performed in a spherical geometry. The disagreement is larger when one considers the evolution of the thickness of the TBL as a function of Ra_H (Fig. 3(b)). First, for $Ra_H \leq 10^4$, the scaling law grossly fails to predict δ_{TBL}. Second, for $10^5 < Ra_H < 10^8$, the fitting of the data with $\beta = -1/4$ is quite poor, and a much better fit is obtained with $\beta_\delta = -0.168$ and $\beta_\delta = -0.151$ for free slip and rigid boundary conditions, respectively. Third, we note a change in the trend of the data at $Ra_H > 10^8$ for rigid boundary conditions. These disagreements confirm that the classical view of the TBL is not able to account for the full dynamics of the convective system.

To be more consistent with our framework, in which the base of the TBL is set at its limit of stability, we use the maximum instantaneous temperature at a given depth rather than an average temperature to define the TBL. From this maximum temperature we construct a "hot temperature" profile, $T_{hot}(z)$, as illustrated in Fig. 1. We then note that the temperature in the TBL increases with depth (i.e., $\partial T_{hot}/\partial z > 0$) and becomes constant (or even slightly decreases) in the convective interior of the fluid underneath the TBL (Fig. 2). We thus use the second spatial derivative of the temperature that marks the change of sign of $\partial T_{hot}/\partial z$ to define the limit between these two zones. We set the base of this Hottest Thermal Boundary Layer (HotTBL) as the first point from the top boundary where the second derivative of the temperature equals zero (in practice where the second derivative is smaller than 1% of its minimum value along the profile).

Fig. 4(a) plots together the temperature difference across the HotTBL, $\Delta T_{TBL} = T_{hot}(z = d - \delta_{TBL})$, determined with the method presented above, and the theoretical law of Eq. (18). The agreement between the numerical results and the theoretical law is excellent. This can be taken as a cross validation of both the theoretical scaling laws and our method of determination of the (Hot)TBL based on the hot temperature profile. We further find that, contrary to previous methods of determination of the TBL, our analytical scaling laws remain valid for the whole range of Ra_H considered. Fig. 4 (b) compares δ_{TBL} obtained in the numerical experiments with the theoretical scaling law of Eq. (19). Here again the agreement is very good, although less impressive because the error bars are higher for δ_{TBL} than for ΔT_{TBL}. This reflects the higher sensitivity of the result to the numerical criterion used to set the HotTBL, an inherent drawback of any method of determination of the TBL thickness.

3.3. The Rayleigh number of the Hottest Thermal Boundary Layer

Our view of the TBL, and the resulting scaling laws, bear important implications for the understanding of the physics of convection through a better description of the internal dynamics of the TBL. In particular, our results may help to solve the long-standing controversy about the value of the local Rayleigh number (Ra_{TBL}) at which the TBL becomes unstable. Early studies (Sharpe and Peltier, 1978; Schubert et al., 1979) considered that Ra_{TBL} was simply $Ra_{H,cr}$, the threshold Rayleigh-Roberts number for the onset of convection. But few years later, Ra_{TBL} was treated as an empirical parameter with no relation with $Ra_{H,cr}$ (Stevenson et al., 1983). More recently numerical experiments by Sotin and Labrosse (1999) showed that Ra_{TBL} was indeed a function of Ra_H, which implied in turn that Ra_{TBL} could not be equal to (constant) $Ra_{H,cr}$. Using our formalism, the definition of the Rayleigh-Roberts number and Eqs. (18) and (19), we predict that the Rayleigh-Roberts number of the HotTBL is

$$Ra_{TBL} = (g\alpha\Delta T_{TBL}\delta_{TBL}^3)/(\kappa\nu) = 0.5\,Ra_{H,cr}. \quad (20)$$

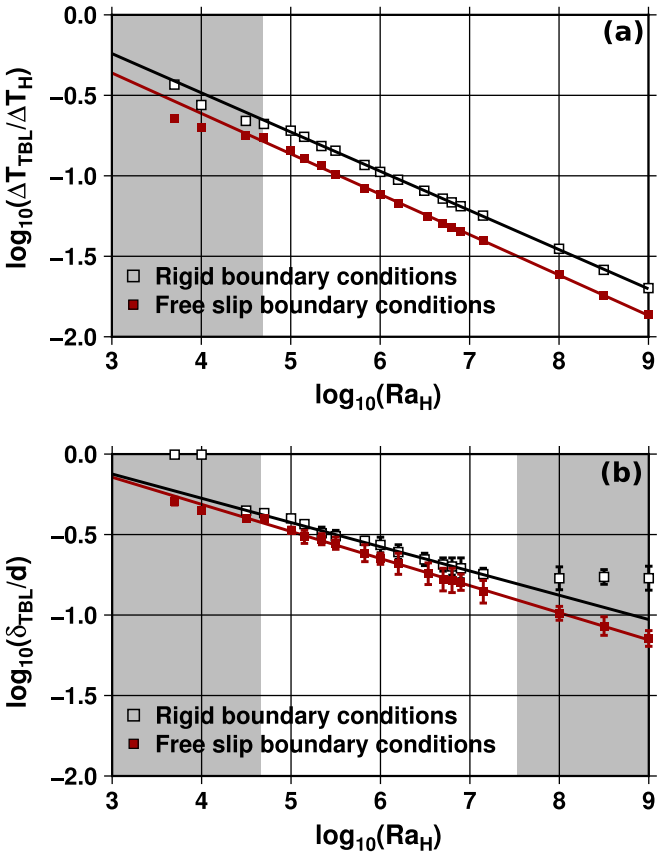

Fig. 3. Evolution of (a) the dimensionless temperature change and (b) the thickness of the thermal boundary layer as a function of the Rayleigh-Roberts number for free slip (red squares) and rigid (black open squares) boundary conditions. The base of the thermal boundary layer is set at the point where the horizontally averaged temperature profile reaches a maximum value. Error bars correspond to temporal variation; they are smaller than the symbol size for ΔT_{TBL}. The solid lines give the best fit of data at Rayleigh-Roberts numbers greater than 10^5. The grey shaded areas correspond to the range of Rayleigh-Roberts numbers where the numerical results do not agree with the scaling laws. (For interpretation of the references to colour in this figure legend, the reader is referred to the web version of this article.)

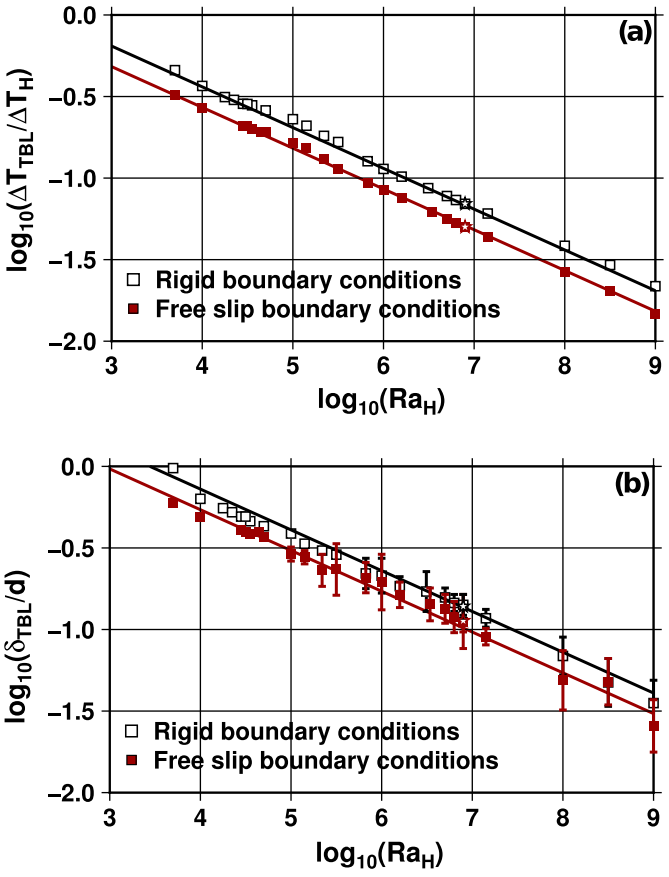

Fig. 4. Evolution of (a) the dimensionless temperature change and (b) the thickness of the thermal boundary layer as a function of the Rayleigh-Roberts number for free slip (red squares) and rigid (black open squares) boundary conditions. The base of the thermal boundary layer is set using the hot temperature profile and the method explained in text. Error bars correspond to temporal variation; they are smaller than the symbol size for ΔT_{TBL}. The solid lines are the theoretical scaling laws defined in text. The two stars correspond to two test cases calculated with non symmetrical mechanical boundary conditions at $\log_{10}(Ra_H) = 5.83$. (For interpretation of the references to colour in this figure legend, the reader is referred to the web version of this article.)

This result demonstrates that the Rayleigh number within the HotTBL is indeed constant hence not a function of Ra_H, and keeps the value reached at the onset of convection (i.e., when $\delta_{TBL} = d$). This is consistent with our view that the TBL is always at the limit of stability, i.e., in a critical state. It is thus likely that the finding of a variable Ra_{TBL} by Sotin and Labrosse (1999) was an artifact due to a non fully consistent definition of the TBL.

As already mentioned, the limit between conduction and convection, hence $Ra_{H,cr}$, depends on the mechanical boundary conditions at the top and at the base of the fluid layer. But the stability of the TBL itself, and the corresponding Ra_{TBL}, are likely to be also affected by the mechanical boundary condition at the base of the HotTBL, i.e., the mechanical interface with the convective interior, which is not known *a priori*. One could expect a mixed condition at this interface, intermediate between a rigid (solid) boundary and a free slip (convective fluid) boundary. In such an intermediate case, the critical Rayleigh number for the HotTBL should then be bracketed by the theoretical values of $Ra_{H,cr}$ for free slip and rigid conditions. We have seen however that this is not the case as Ra_{TBL} keeps the same value as the one calculated at the onset of convection (whatever the Ra_H of the system) for a given fixed boundary condition (either rigid or free slip). In order better to understand this rather counter intuitive result, we carried out additional numerical simulations at high Ra_H with asymmetrical mechanical boundary conditions at the top and at the bottom of the system (Fig. 4). We find that the HotTBL properties (both temperature and thickness) for asymmetric boundary conditions are the same as the ones obtained for symmetrical boundary conditions. This implies that Ra_{TBL} in the asymmetrical cases has the same value as in a symmetrical system with the same top boundary condition. Hence that the effective mechanical condition "seen" at the base of the HotTBL is the same as the one imposed at the upper boundary. This result implies in turn that the dynamics of a volumetrically heated convective system depends only on Ra_H and on the top mechanical boundary condition.

4. Application to the onset of partial melting in exoplanets

The scaling laws established in the previous section provide a robust description of the thermal structure of a purely internally heated convective system based on the characteristics of the thermal boundary layer. We will now show how such scaling laws can be used to assess the occurrence of partial melting in exoplanets. As a first step we will compare the predictions of the scaling laws with the results of a 3D spherical numerical model of convection in the mantle of the Moon (Laneuville et al., 2013).

4.1. Thermal state of the Moon's mantle

The traces of past volcanic activity at the surface of the Moon are strongly asymmetric. Most of the lunar maria are located on the nearside and the age of volcanism is different on the two sides: dating based on lunar samples and crater counting techniques gives ages between 1 and 4 Ga for the nearside (Hiesinger et al., 2003) and 2.5–3 Ga for the farside (Haruyama et al., 2009). This dichotomy is related to an enrichment in radioactive isotopes in the nearside relative to the farside (Lawrence et al., 1998), which yields larger interior temperatures and favors volcanism. The degree of enrichment is constrained from the samples of Apollo 15 mission (Korotev, 2000), and observations of lunar maria and surface measurements of thorium concentrations (Lawrence et al., 2003), which indicate a more or less circular shallow enriched zone with a diameter of ~80° (Jolliff et al., 2000).

Laneuville et al. (2013) conducted simulations of thermochemical convection in 3D spherical geometry in a stagnant-lid regime to quantify the impact of the enriched zone on the thermal evolution of the Moon. They systematically studied the effect of the model parameters, including the location, size and degree of enrichment of the zone. They then selected the model parameters that best fit the observations.

An important by-product of Laneuville et al. (2013)'s results in the framework of the present study, is to show that the heat flux at the base of the lunar mantle can be neglected compared to radioactive internal heating. This allows us to compare their results to the predictions of our scaling laws for a rigid surface and using their choice of best-fitting parameters (Table 3). However, important differences between our scaling laws and the model of Laneuville et al. (2013) have to be taken into account before comparing the results of the two approaches.

First, we have to take into account the sphericity of the Moon's mantle. To that aim we follow Deschamps et al. (2012) and correct the Rayleigh-Roberts number using a geometric factor a_f,

$$Ra_{VH} = a_f Ra_H \tag{21}$$

where a_f is calculated from

$$a_f = \frac{1}{3}\left[1 + \frac{R_c}{R_c + d_m} + \left(\frac{R_c}{R_c + d_m}\right)^2\right], \tag{22}$$

with R_c the core radius and d_m the depth of the mantle. As in Deschamps et al. (2012) we also introduce a modified temperature scale,

$$\Delta T_{VH} = a_f \Delta T_H. \tag{23}$$

Using the corrected Rayleigh-Roberts number and temperature scale, our scaling laws (18) and (19) are then written for a spherical geometry as

$$\Delta T_{TBL}/\Delta T_H = 0.5\, a_f^{3/4} \left(Ra_{H,cr}/Ra_H\right)^{1/4}, \tag{24}$$

$$\delta_{TBL}/d = a_f^{-1/4} \left(Ra_{H,cr}/Ra_H\right)^{1/4}. \tag{25}$$

Second, we need to consider the potential implications of heterogeneous heating. In the Moon's mantle, the volumetric heating may come from both the decay of radioactive isotopes and secular cooling. We used the surface heat flux ϕ obtained in the model of Laneuville et al. (2013), 25 mW m^{-2} in the nearside and 10 mW m^{-2} in the farside, to derive the corresponding amount of internal heating in each hemisphere using $H = \phi/d_m$. Furthermore, Laneuville et al. (2013) consider a vertically heterogeneous distribution of internal heating, with, in the two hemispheres, a 40 km crust ≈ 20 times enriched in heat producing elements compared to the mantle, and, in the nearside only, an additional 10 km thick enriched layer located at the base of the crust. Here we thus consider a 50 km thick layer ≈ 60 times enriched in heat producing elements relative to the mantle (which satisfies the surface heat flux constraint) for the nearside, whereas we consider only the 40 km thick crust for the farside. To remain fully consistent with our approach, we further calculate the new conductive profile for the two considered vertical distributions of heat production (see Supplementary Material). We then compute the new value of the critical Rayleigh-Roberts number, that we found to be identical to the homogeneous heating case. The resulting new expressions for the dimensionless coefficients of the scaling laws are $C_T^* = 0.540\, Ra_{H,cr}^{1/4}$ and $C_T^* = 0.508\, Ra_{H,cr}^{1/4}$ for the nearside and farside, respectively, and $C_\delta^* = Ra_{H,cr}^{1/4}$ in the two cases.

Table 3
Parameters of the Moon's model.

Symbol	Description	Value
R_p	Planet radius	1740 km
R_c	Core radius	390 km
d_m	Mantle depth	1350 km
a_f	Geometric factor	0.425
T_{surf}	Surface temperature	250 K
g_m	Acceleration of gravity	1.62 m s^{-2}
η_m	Viscosity	5 10^{22} Pa s
λ_m	Thermal conductivity	3.0 W m^{-1} K^{-1}
κ_m	Thermal diffusivity	10^{-6} m^2 s^{-1}
α_m	Thermal expansion coefficient	2 10^{-5} K^{-1}
ρ_m	Density	3400 kg m^{-3}
H_m	Radioactive Heating rate of the mantle	7 10^{-9} W m^{-3}
H_f	Bulk heating rate for the farside	1.66 10^{-8} W m^{-3}
H_n	Bulk heating rate for the nearside	4.15 10^{-8} W m^{-3}

We used the laws given in Eqs. (24) and (25) with the coefficients C_T^* and C_δ^* corresponding to the heterogeneous distribution of internal heating to estimate the internal temperature of the Moon ($T_{int} = T_{surf} + \Delta T_{TBL}$) as well as the thickness of the TBL (δ_{TBL}) in the two hemispheres. We consider the two hemispheres as independent, as Laneuville et al. (2013) has shown that the two convective systems hardly interfere with each other, and we decrease the nearside mantle viscosity by one order of magnitude to account for the effect of the higher temperature induced by the enriched zone. For the nearside we obtain,

$$T_{int} = 1767 \text{ K}, \tag{26}$$

$$\delta_{TBL} = 354 \text{ km}, \tag{27}$$

and for the farside,

$$T_{int} = 1529 \text{ K}, \tag{28}$$

$$\delta_{TBL} = 793 \text{ km}. \tag{29}$$

The predictions of the scaling laws are compared in Fig. 5 with the temperature profiles found by Laneuville et al. (2013). The good agreement between the two results shows that our theoretical scaling laws can be applied to convective mantle of spherical planetary bodies. We will show now how this approach can be applied to the less well constrained and more challenging case of exoplanets.

4.2. Thermal boundary layers of exoplanets

Our scaling laws give the temperature at the base of the HotTBL for internally heated convective systems. By comparing this temperature to the solidus of the planetary material it is then possible to assess the occurrence of partial melting. Here we propose to illustrate this approach when applied to a silicate sphere that can represent either a coreless terrestrial planet, a mantle of a planet with a small heat flux coming from the core, or the rocky core of an ice giant.

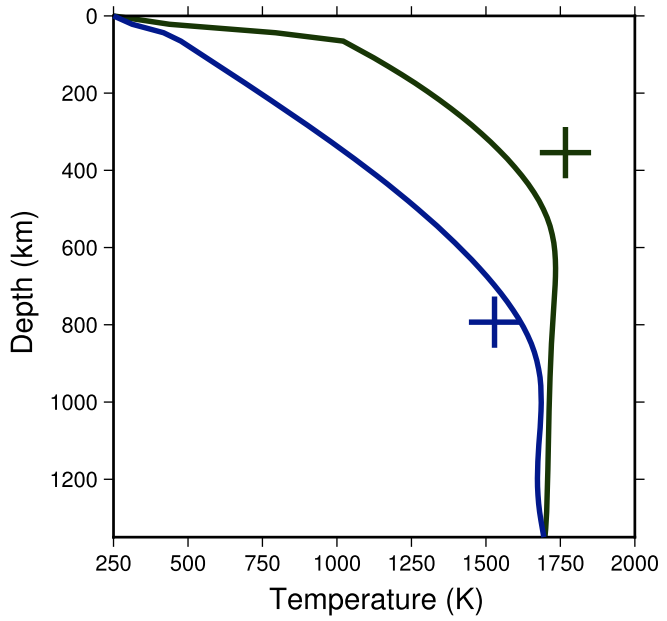

Fig. 5. Temperature profiles of the nearside (green line) and farside (blue line) of the Moon obtained by Laneuville et al. (2013) (Fig. 5). The two crosses are the base of the TBL predicted by our scaling laws (Eqs. (24) and (25)) for the nearside (green) and farside (blue). (For interpretation of the references to colour in this figure legend, the reader is referred to the web version of this article.)

To compute the effective temperature at the base of the TBL in the context of exoplanet habitability, we will take T_{surf} = 300 K, in order to ensure the presence of liquid water as usually done in the definition of the "conventional" habitable zone (Seager, 2013). The top temperature of the rocky core of an ice giant is difficult to constrain and may be lower. However, the presence of a subsurface ocean, observed in several icy satellites, suggests a temperature at the interface between the core and the icy mantle of about 250 K (Khurana et al., 1998; Kivelson et al., 2002; Lorenz et al., 2008; Rubie et al., 2015).

For a given surface temperature, our scaling laws can be used to estimate directly the temperature at the base of the HotTBL in an isoviscous fluid. However, in the case of large variation of viscosity with temperature such as expected in planetary mantles, the presence of a viscous lid above the HotTBL has to be taken into account. We thus consider that in a planetary mantle the temperature T_{int} at the base of the HotTBL is equal to the surface temperature, plus the temperature increase across the viscous lid, ΔT_{lid}, plus the temperature increase across the HotTBL, ΔT_{TBL}. The depth of the base of the HotTBL is the sum of the thickness of the viscous lid, δ_{lid}, and of the HotTBL, δ_{TBL}. To assess the occurrence of partial melting at the base of the HotTBL it is thus necessary to infer ΔT_{lid} and δ_{lid}. Previous studies (Solomatov and Moresi, 2000; Deschamps and Lin, 2014) have shown that the viscous lid can be taken as a conductive layer, which introduces the following relationship between ΔT_{lid} and δ_{lid}:

$$\Delta T_{lid} = \frac{a_f H \delta_{lid}^2}{2\lambda}, \tag{30}$$

and which leaves δ_{lid} as the last unknown parameter. But the thickness of the viscous lid depends both on the rheological law and on the internal temperature of the system, and there is no direct method to obtain it.

To characterize the viscous lid, we use the "viscous" temperature scale, ΔT_η, first defined by Davaille and Jaupart (1993) as

$$\Delta T_\eta = \frac{\eta(T_{int})}{\mathrm{d}\eta/\mathrm{d}T(T_{int})}, \tag{31}$$

which explicitly introduces the law giving the variation of viscosity with temperature. Grasset and Parmentier (1998) further showed that the viscous temperature scale is proportional to the temperature jump across the TBL,

$$\Delta T_\eta = \frac{1}{2.23}\Delta T_{TBL}, \tag{32}$$

which, once combined with Eq. (31), introduces an additional (non linear) relationship between T_{int} and ΔT_{TBL} that closes the system.

To solve the system, we start from a (large) estimate of the internal temperature, say T^*_{int}=2500 K. From T^*_{int} (and knowing the rheological law, see below) we estimate ΔT_η from Eq. (31), then ΔT_{TBL} from Eq. (32), and finally $\Delta T_{lid} = T*_{int} - T_{surf} - \Delta T_{TBL}$. From ΔT_{lid} we obtain δ_{lid} (Eq. (30)) which in turn is used to calculate the effective Rayleigh-Roberts number for the convecting fluid below the viscous lid:

$$Ra^*_H = a_f \frac{\rho\alpha g H (d-\delta_{lid})^5}{\lambda\kappa\eta(T^*_{int})}. \tag{33}$$

Using Ra^*_H in our scaling law gives a new estimate of ΔT_{TBL} which is the same as the one given by Eq. (32) only if T^*_{int} is the correct internal temperature. We thus iteratively change the values of T^*_{int} until the two estimates of ΔT_{TBL} differ by less than 0.1 K.

4.3. Partial melting in exoplanets

In planetary bodies, partial melting occurs when the temperature of the material reaches its solidus. Because the slope of the variation of the solidus temperature with depth is smaller than that of the temperature in a convective system, partial melting preferentially occurs at the base of the TBL. We therefore consider that partial melting starts when the temperature at the base of the HotTBL (T_{int}) reaches the solidus, i.e.,

$$T_{int} \geqslant T_{solidus}(r = d - \delta_{TBL}), \tag{34}$$

where $T_{solidus}$ is the temperature of the solidus at the pressure (or radius) corresponding to the base of the HotTBL. In the following we will use a solidus profile compiled from different experimental studies of terrestrial peridotites at pressures ranging up to 140 GPa (Hirschmann, 2000; Zhang and Herzberg, 1994; Andrault et al., 2011).

For a given set of physical properties (see below), threshold conditions for partial melting to occur can be expressed as a function of the planet radius R and the heating rate H. For a given H, the radius of the planet is key in determining the Rayleigh-Roberts number. First, the radius can be used to set the acceleration of gravity, $g = GM/R^2$, with G the gravitational constant and M the mass of the planet. To express the results of the model as a function of the radius of the planet only we further use the mass-radius relationship obtained by Valencia et al. (2006) for Earth-like planets,

$$\frac{R}{R_T} = \left(\frac{M}{M_T}\right)^{0.27}, \tag{35}$$

where R_T and M_T are the radius and mass of the Earth, respectively. This relationship has been shown to remain applicable for different planet compositions (Sotin et al., 2007) as well as for coreless planets (Elkins-Tanton and Seager, 2008). Last, we estimate the depth of the mantle of differentiated planets from the size of their core, R_c, estimated from Valencia et al. (2006),

$$d = R - R_c = R - 3.5\,10^3 \left(\frac{R}{R_T}\right)^{0.926}, \tag{36}$$

where d, R and R_c are in kilometers.

If the radius of an exoplanet can be deduced from observations, estimates of the rate of internal heating rely on indirect arguments. In a terrestrial planet, volumetric heating is mainly due to the decay of radioactive isotopes, which itself decreases as a function of time and depends on the half-life of the considered isotopes. For example, ^{26}Al, which has a half-life smaller than 1 Myr, plays a role only on the early ($\leqslant$x10 Myr) thermal evolution of a planetary body, whereas long life isotopes such as ^{235}U are important in old and cold planets. As already mentioned, the progressive loss of the primordial heat is equivalent to an additional source of internal heat. Lebrun et al. (2013) studied the early thermal evolution of Earth taking into account the release of the primordial heat and short-lived radioactive isotopes. They found that the surface heat flux few millions years after the Earth formation was 10^2 times higher than today. Combined with the estimates of internal heating in the present-day Earth (10^{-8}–10^{-7} W m^{-3}; McDonough and Sun, 1995; Javoy and Kaminski, 2014; Jellinek and Jackson, 2015) this suggests an upper bound for internal heating in young planets of 10^{-5} W m^{-3}. Unterborn et al. (2015) studied Th abundances in 14 solar twins and analogs, and found values ranging between 0.59 and 2.51 times the Th concentration of the Sun. All things being equal we used these same proportions to estimate possible Th content of exoplanets relative to the Earth. We then calculate their total heat production using terrestrial U/Th and K/U ratios. We obtain a total range of 10^{-9} to 10^{-4} W m^{-3} which includes the case of young planets discussed above.

We now consider the possible range of physical properties for the silicate mantle of terrestrial exoplanets. As explained above, the evolution of viscosity with temperature is key in determining the internal temperature of the system. Here we take the same law as Ricard and Zhong (2006),

$$\eta(T) = \eta_0 \exp\left(\frac{E}{R_m T} - \frac{E}{R_m T_0}\right), \tag{37}$$

with $E = 310^5$ J mol^{-1} the activation energy, $R_m = 8.314$ J mol^{-1} K^{-1} the universal gas constant and $T_0 = 1600$ K the reference temperature at which $\eta = \eta_0 = 10^{21}$ Pa s^{-1} (Karato and Wu, 1993). Once T_{int} has been estimated, this law gives the viscosity of the convective system below the viscous lid, $\eta(T_{int})$. Values of the other model parameters are given in Table 4 based on Tackley et al. (2013) estimations of material properties at depth.

The final step for the construction of the regime diagram is the comparison of T_{int} with the solidus temperature at the base of the TBL, which itself depends on the pressure at that depth. To obtain the solidus temperature, we relied on the simple analytical expression for the pressure profile $P(r)$ in planetary mantles proposed by Zeng and Jacobsen (2016),

$$P(r) = P_{CMB}\frac{\ln(R/r)}{\ln(R/R_c)}, \tag{38}$$

with P_{CMB} the pressure at the planet core mantle boundary. We used Eq. (36) to estimate R_c and the results of Sotin et al. (2007) to estimate P_{CMB} (in GPa) as

$$P_{CMB} = 136\,(M/M_T). \tag{39}$$

For coreless planets, we use the approximate solution developed by Seager et al. (2007),

$$P(r) = \frac{3G}{8\pi}\frac{M^2}{R^6}\left(R^2 - r^2\right). \tag{40}$$

Fig. 6(a) shows the regime diagram for the occurrence of partial melting as a function of R and H in a coreless planet. We observe two trends in the evolution of the heating rate (H_{melt}) at which partial melting occurs. For R smaller than $\approx 2\ 10^3$ km, H_{melt} decreases with increasing radius, whereas H_{melt} increases with R for radii larger than $\approx 2\ 10^3$ km. The decrease of H_{melt} with increasing radius in "small planets" ($R < 2\ 10^3$ km) is actually not to be interpreted based on our scaling laws for convection: in these planets the solidus is crossed by the stable conductive temperature profile. Because the conductive temperature ΔT_H scales as HR^2, while the increase of the solidus temperature is relatively small over the pressure range relevant for small planets, H_{melt} is expected to decrease as R^{-2}, as observed in the regime diagram. In "Earth-like" planets ($R > 2\ 10^3$ km), the increase of H_{melt} with the planet radius can be interpreted based on the scaling laws. First our scaling laws predicts that the TBL temperature scales as $\Delta T_H Ra_H^{-1/4}$, i.e., as $H^{3/4}R^{3/4}$. Second, the solidus temperature will scale as the lithostatic pressure at the base of the TBL, given at first order by the product $\rho g \delta_{TBL}$ which itself scales as $H^{-1/4}R^{1.45}$ according to our scaling law and the variation of g with R deduced from Eq. (36). Combining the two temperature scales we predict that H_{melt} increases as $R^{0.7}$, in good agreement with the regime diagram.

The evolution of H_{melt} in differentiated planets, showed in Fig. 6 (b), is almost the same as in coreless planets, and the interpretations given above remain valid. The main difference between the two diagrams is the systematically higher value of H_{melt} in the differentiated planet in the conductive regime (i.e., $R < 2\ 10^3$ km). This can be readily interpreted as the difference between a coreless planet where the convective fluid has the total thickness R, and a planet with a core where the convective fluid has the thickness of the mantle only, $d = R - R_c$. Because the temperature scales as the square of the thickness of the convective fluid, a smaller thickness implies a higher heating rate to reach the solidus. For $R > 2\ 10^3$ km, H_{melt} is first larger in differentiated planets than in coreless planets and then becomes smaller. This is due to the faster evolution of H_{melt} in coreless planets where it scales as $R^{0.7}$ than in differentiated planets where it scales as $d^{0.7}$ (with $d < R$).

We also show in Fig. 6 the typical estimates of present day heating rate in the Earth (with 10^{-8} W m^{-3} as a lower bound) as well as the higher estimate for Earth-like planets deduced from Unterborn et al. (2015) ($5\ 10^{-8}$ W m^{-3}). Taking into account reasonable estimates of the likely contribution of secular cooling ($\approx$ equivalent to radioactive heating based on the example of the Earth), and the evolution of radioactive heating in planets after the formation of their galaxy (Frank et al., 2014), we can conclude that partial melting is expected in exoplanets younger than the Earth. In old planets on the other hand, the decrease of both secular cooling and heating rate will make partial melting less likely, which will decrease the probability of a long-term atmosphere.

Table 4
Parameters used for the application of the scaling laws to exoplanets.

Symbol	Unit	Description	Minimum value	Maximum value	Assumed value
ρ	kg m^{-3}	Density	3300	11,000	4000
α	K^{-1}	Thermal expansion coefficient	$2\ 10^{-6}$	$3\ 10^{-5}$	$3\ 10^{-5}$
λ	W m^{-1} K^{-1}	Thermal conductivity	3	30	3
κ	m^2 s^{-1}	Thermal diffusivity	$7\ 10^{-7}$	$2\ 10^{-6}$	$7\ 10^{-7}$

The minimum and maximum values of the parameters represent their range of variation from the surface value to their value at depth taken from (Tackley et al., 2013).

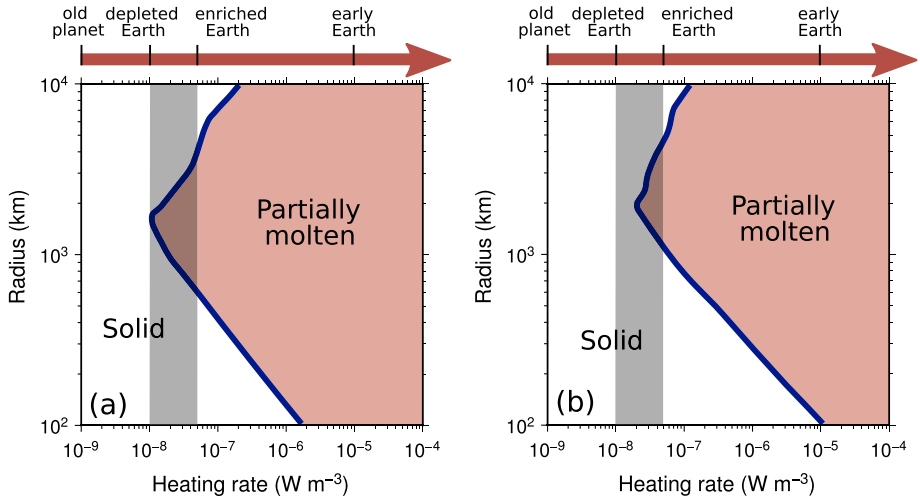

Fig. 6. Regime diagram giving the conditions for partial melting to occur within (a) coreless planets and (b) differentiated planets, as a function of their radius (R) and heating rate (H). The blue lines give the threshold heating rate H_{melt} at which the base of the TBL reaches the solidus. The grey shaded areas give the present day estimates for radioactive heating in the Earth and in Earth-like exoplanets (Unterborn et al., 2015). In addition, we report at the top of each panels some typical heating rates for planets at different ages (McDonough and Sun, 1995; Lebrun et al., 2013; Laneuville et al., 2013; Frank et al., 2014). (For interpretation of the references to colour in this figure legend, the reader is referred to the web version of this article.)

Water is not the only liquid environment that may allow for the apparition and development of life. Considering other candidates than water will change the definition of the habitable zone and the range of surface temperature considered (Seager, 2013). To test the influence of surface temperature on the occurrence of partial melting, we performed additional calculations with T_{surf} ranging from 0 K to 800 K. We found a rather small impact when varying this parameter. For example, for $R = 10^4$ km, H_{melt} is 4 10^{-7} W m^{-3} at 0 K and 1.1 10^{-7} W m^{-3} at 800 K, whereas for $R = 10^2$ km, H_{melt} is 2.3 10^{-6} W m^{-3} and 8 10^{-7} W m^{-3} for T_{surf} = 0 K and 800 K, respectively. The interpretation of the result is rather straightforward: an increase of surface temperature increases the internal temperature and moves the hot profile closer to the solidus thus making partial melting easier.

5. Conclusion

In the present study, we have established purely theoretical scaling laws giving the thermal structure of a volumetrically heated system as a function of the Rayleigh-Roberts and of the surface mechanical condition (free slip or no-slip) only. Because they do not introduce any empirical fitting parameters, these laws provide a robust framework that can be applied to a large diversity of natural systems. We have shown for example that they successfully predict the thermal structure of the Moon's mantle. Combining the scaling laws with experimental solidus profiles in terrestrial planets, as well as reasonable estimates of their mantle material properties, we have built a regime diagram predicting the occurrence of partial melting as a function of the radius of the planet, and of the heating rate. We conclude that Earth-like planets located in the habitable zone and younger than the Earth are able to generate and maintain an atmosphere through partial melting and volcanism. Both the reduction of secular cooling and the decrease of radioative heating as a function of time in old planets make them less likely to be in the partial melting regime. The present results could be enlarged to the case of the mantle of icy planetary bodies heated by tidal dissipation. The estimates of tidal heating is however a complex and non linear problem that requires important numerical resources. The approach based on scaling laws can provide a rather efficient and robust way to tackle this problem.

Acknowledgements

We thank Louis Moresi and two anonymous reviewer for their thorough and constructive comments that helped us to produce a much improved paper. We also thank Mark Jellinek for his editorial handling of the manuscript. The interpretation of the results benefited from discussions with Stéphane Labrosse, Frédéric Deschamps, Alexandre Fournier and Matthieu Laneuville. We would like to thank Angela Limare, Loic Fourel, Claude Jaupart and Cinzia Farnetani for very useful discussions on convection in internally heated systems. This work was supported by the TERRA-MWH project (ANR-11-ISO4-0004) and by the program PNP of the INSU-CNRS. Numerical computations were performed on the SCAPAD platform, IPGP, France and using HPC resources from GENCI-IDRIS (Grant 2013-047033).

Appendix A. Supplementary data

Supplementary data associated with this article can be found, in the online version, at http://dx.doi.org/10.1016/j.pepi.2017.02.001.

References

Amit, H., Aubert, J., Hulot, G., Olson, P., 2008. A simple model for mantle-driven flow at the top of Earth's core. Earth Planets Space 60, 845–854.
Andrault, D., Bolfan-Casanova, N., Lo Nigro, G., Bouhifd, M.A., Garbarino, G., Mezouar, M., 2011. Solidus and liquidus profiles of chondritic mantle: Implication for melting of the Earth across its history. Earth Planet. Sci. Lett. 304, 251–259.
Badro, J., Brodholt, J.P., Piet, H., Siebert, J., Ryerson, F.J., 2015. Core formation and core composition from coupled geochemical and geophysical constraints. Proc. Nat. Acad. Sci. U.S.A. 112, 12310–12314.
Bakos, G., Noyes, R.W., Kovacs, G., Stanek, K.Z., Sasselov, D.D., Domsa, I., 2004. Wide-field millimagnitude photometry with the HAT: a tool for extrasolar planet detection. Publ. Astron. Soc. Pac. 116, 266–277.
Basri, G., Borucki, W.J., Koch, D., 2005. The kepler mission: a wide-field transit search for terrestrial planets. New Astron. Rev. 49, 478–485.
Behounkova, M., Tobie, G., Choblet, G., Cadek, O., 2011. Tidally induced thermal runaways on extrasolar earths: impact on habitability. Astrophys J 728, 89–98.
Chandrasekhar, S., 1961. Hydrodynamic and Hydromagnetic Stability. Clarendo Press, New York.
Choblet, G., Parmentier, E.M., 2009. Thermal convection heated both volumetrically and from below: implications for predictions of planetary evolution. Phys. Earth Planet. Int. 173, 290–296.
Cockell, C., Bush, T., Bryce, C., Direito, S., Fox-Powell, M., Harrison, J., Lammer, H., Landenmark, H., Martin-Torres, J., Nicholson, N., Noack, L., O'Malley-James, J.,

Payler, Rushby, A., Samuels, T., Schwendner, P., Wadsworth, J., Zorzano, M., 2016. Habitability: a review. Astrobiology 16, 89–117.
Davaille, A., Jaupart, C., 1993. Transient high-Rayleigh-number thermal convection with large viscosity variation. J. Fluid Mech. 253, 141–166.
Deschamps, F., Lin, J.R., 2014. Stagnant lid convection in 3D-Cartesian geometry: scaling laws and applications to icy moons and dwarf planets. Phys. Earth Planet. Int. 229, 40–54.
Deschamps, F., Yao, C., Tackley, P.J., Sanchez-Valle, C., 2012. High Rayleigh number thermal convection in volumetrically heated spherical shells. J. Geophys. Res. 117, E09006.
Elkins-Tanton, L.T., Seager, S., 2008. Coreless terrestrial exoplanets. Astrophys. J. 688, 628–635.
Frank, E.A., Meyer, B.S., Mojzsis, S.J., 2014. A radiogenic heating evolution model for cosmochemically Earth-like exoplanets. Icarus 243, 274–286.
Grasset, O., Parmentier, E.M., 1998. Thermal convection in a volumetrically heated, infinite Prandtl number fluid with strongly temperature-dependent viscosity: implications for planetary thermal evolution. J. Geophys. Res. 103, 18171–18181.
Grossmann, S., Lohse, D., 2000. Scaling in thermal convection: a unifying theory. J. Fluid Mech. 407, 27–56.
Grossmann, S., Lohse, D., 2001. Thermal convection for large Prandtl numbers. Phys. Rev. Lett. 86, 3316–3319.
Haruyama, J., Ohtake, M., Matsunaga, T., Morota, T., Honda, C., Yokota, Y., Abe, M., Ogawa, Y., Miyamoto, H., Iwasaki, A., Pieters, C.M., Asada, N., Demura, H., Hirata, N., Terazono, J., Sasaki, S., Saiki, K., Yamaji, A., Toril, M., Josset, J.L., 2009. Long-lived volcanism on the lunar farside revealed by SELENE terrain camera. Science 323, 905–908.
Hiesinger, H., Head III, J.W., Wolf, U., Jaumann, R., Neukum, G., 2003. Ages and stratigraphy of mare basalts in oceanus procellarum, mare nubium, mare cognitum, and mare insularum. J. Geophys. Res. 108, 5065.
Hirschmann, M.M., 2000. Mantle solidus: Experimental constraints and the effects of peridotite composition. Geochemistry Geophysics Geosystems 1, 2000GC000070.
Howard, L.N., 1966. Convection at high Rayleigh number. In: Gortler, H. (Ed.), Proceedings of the 11th International Congress on Applied Mechanics. Springer-Verlag, New York, pp. 1109–1115.
van Hunen, J., Zhong, S., 2003. New insight in the Hawaiian plume swell dynamics from scaling law. Geophys. Res. Lett. 30, 1785.
Jaupart, C., Mareschal, J.C., 2011. Heat Generation and Transport in the Earth. Cambridge University Press, Cambridge.
Javoy, M., Kaminski, E., 2014. Earth's uranium and thorium content and geoneutrinos fluxes based on enstatite chondrites. Earth Planet. Sci. Lett. 407, 1–8.
Jellinek, A.M., Jackson, M.G., 2015. Connections between the bulk composition, geodynamics and habitability of Earth. Nat. Geosci. 8, 587–593.
Jolliff, B.L., Gillis, J.J., Haskin, L.A., Korotev, R.L., Wieczorek, M.A., 2000. Major lunar crustal terranes: surface expressions and crust-mantle origins. J. Geophys. Res.: Planets 105, 4197–4216.
Karato, S.I., Wu, P., 1993. Rheology of the upper mantle: a synthesis. Science 260, 771–778.
Ke, Y., Solomatov, V.S., 2009. Coupled core-mantle thermal evolution of early Mars. J. Geophys. Res.: Planets 114, E07004.
Khurana, K.K., Kivelson, M.G., Stevenson, D.J., Schubert, G., Russell, C.T., Walker, R.J., Polanskey, C., 1998. Induced magnetic fields as evidence for subsurface oceans in Europa and Callisto. Nature 395, 777–780.
Kivelson, M.G., Khurana, K.K., Volwerk, M., 2002. The permanent and inductive magnetic moments of ganymede. Icarus 157, 507–522.
Korotev, R.L., 2000. The great lunar hot spot and the composition and origin of the Apollo mafic (LKFM) impact-melt breccias. J. Geophys. Res.: Planets 105, 4317–4345.
Krishnamurti, R., 1968. Finite amplitude convection with changing mean temperature. Part 1. Theory. J. Fluid Mech. 33, 445–455.
Labrosse, S., Hernlund, J.W., Coltice, N., 2007. A crystallizing dense magma ocean at the base of the Earth's mantle. Nature 450, 866–869.
Labrosse, S., Poirier, J.P., Le Mouël, J.L., 2001. The age of the inner core. Earth Planet. Sci. Lett. 190, 111–123.
Laneuville, M., Wieczorek, M.A., Breuer, D., Tosi, N., 2013. Asymmetric thermal evolution of the Moon. J. Geophys. Res. Planets 118, 1435–1452.
Lawrence, D.J., Elphic, R.C., Feldman, W.C., Prettyman, T.H., Gasnault, O., Maurice, S., 2003. Small-area thorium features on the lunar surface. J. Geophys. Res. Planets 108, 5102.
Lawrence, D.J., Feldman, W.C., Barraclough, B.L., Binder, A.B., Elphic, R.C., Maurice, S., Thomsen, D.R., 1998. Global elemental maps of the moon: the lunar prospector gamma-ray spectrometer. Science 281, 1484–1489.
Lebrun, T., Massol, H., Chassefière, E., Davaille, A., Marcq, E., Sarda, P., Leblanc, F., Brandeis, G., 2013. Thermal evolution of an early magma ocean in interaction with the atmosphere. J. Geophys. Res. Planets 118, 1155–1176.
Limare, A., Vilella, K., Di Giuseppe, E., Farnetani, C., Kaminski, E., Surducan, E., Surducan, V., Neamtu, C., Fourel, L., Jaupart, C., 2015. Microwave-heating laboratory experiments for planetary mantle convection. J. Fluid Mech. 1565, 14–18.
Lorenz, R.D., Stiles, B.W., Kirk, R.L., Allison, M.D., del Marmo, P.P., Iess, L., Lunine, J.I., Ostro, S.J., Hensley, S., 2008. Titan's rotation reveals an internal ocean and changing zonal winds. Science 319, 1649–1651. http://dx.doi.org/10.1126/science.1151639.
McDonough, W.F., Sun, S.S., 1995. The composition of the Earth. Chem. Geol. 120, 223–253.
McKenzie, D.P., Weiss, N., 1975. Speculations on the thermal and tectonic history of the Earth. Geophys. J. Roy. Astron. Soc. 42, 131–174.
Mullally, F., Coughlin, J.L., Thompson, S.E., Rowe, J., Burke, C., Latham, D.W., Batalha, N.M., Bryson, S.T., Christiansen, J., Henze, C.E., Ofir, A., Quarles, B., Shporer, A., Van Eylen, V., Van Laerhoven, C., Shah, Y., Wolfgang, A., Chaplin, W.J., Xie, J.W., Akeson, R., Argabright, V., Bachtell, E., Barclay, T., Borucki, W.J., Caldwell, D.A., Campbell, J.R., Catanzarite, J.H., Cochran, W.D., Duren, R.M., Fleming, S.W., Fraquelli, D., Girouard, F.R., Haas, M.R., Hełminiak, K.G., Howell, S.B., Huber, D., Larson, K., Gautier, III, T.N., Jenkins, J.M., Li, J., Lissauer, J.J., McArthur, S., Miller, C., Morris, R.L., Patil-Sabale, A., Plavchan, P., Putnam, D., Quintana, E.V., Ramirez, S., Silva Aguirre, V., Seader, S., Smith, J.C., Steffen, J.H., Stewart, C., Stober, J., Still, M., Tenenbaum, P., Troeltzsch, J., Twicken, J.D., Zamudio, K.A., 2015. Planetary Candidates Observed by Kepler. VI. Planet Sample from Q1–Q16 (47 Months). Astrophys. J. Suppl. Ser. 217, 31.
Parmentier, E.M., Sotin, C., 2000. Three-dimensional numerical experiments on thermal convection in a very viscous fluid: implications for the dynamics of a thermal boundary layer at high Rayleigh number. Phys. Fluids 12, 609–617.
Pollacco, D.L., Skillen, I., Collier Cameron, A., Christian, D.J., Hellier, C., Irwin, J., Lister, T.A., Street, R.A., West, R.G., Anderson, D., Clarkson, W.I., Deeg, H., Enoch, B., Evans, A., Fitzsimmons, A., Haswell, C.A., Hodgkin, S., Horne, K., Kane, S.R., Keenan, F.P., Maxted, P.F.L., Norton, A.J., Osborne, J., Parley, N.R., Ryans, R.S.I., Smalley, B., Wheatley, P.J., Wilson, D.M., 2006. The WASP project and the SuperWASP cameras. Publ. Astron. Soc. Pac. 118, 1407–1418.
Ricard, Y., Richards, M., Lithgow-Bertelloni, C., Le Stunff, Y., 1993. A geodynamic model of mantle density heterogeneity. J. Geophys. Res. Solid Earth 98, 21895–21909.
Roberts, J.H., Zhong, S., 2006. Degree-1 convection in the Martian mantle and the origin of the hemispheric dichotomy. J. Geophys. Res. Planets 111, E06013.
Roberts, P.H., 1967. Convection in horizontal layers with internal heat generation. Theory J. Fluid Mech. 30, 33–49.
Rubie, D.C., Jacobson, S.A., Morbidelli, A., O'Brien, D.B., Young, E.D., de Vries, J., Nimmo, F., Palme, H., Frost, D.J., 2015. Accretion and differentiation of the terrestrial planets with implications for the compositions of early-formed Solar System bodies and accretion of water. Icarus 248, 89–108.
Saur, J., Duling, S., Roth, L., Jia, X., Strobel, D.F., Feldman, P.D., Christensen, U.R., Retherford, K.D., McGrath, M.A., Musacchio, F., Wennmacher, A., Neubauer, F.M., Simon, S., Hartkorn, O., 2015. The search for a subsurface ocean in ganymede with hubble space telescope observations of its auroral ovals. J. Geophys. Res. Space Phys. 120, 1715–1737.
Schubert, G., Cassen, P., Young, R.E., 1979. Subsolidus convective cooling histories of terrestrial planets. Icarus 38, 192–211.
Seager, S., 2013. Exoplanet habitability. Science 340, 577–581.
Seager, S., Kuchner, M., Hier-Majumder, C.A., Militzer, B., 2007. Mass-radius relationships for solid exoplanets. Astrophys. J. 669, 1279–1297.
Sharpe, H., Peltier, W.R., 1978. Parameterized mantle convection and the Earth's thermal history. Geophys. Res. Lett. 5, 737–740.
Solomatov, V.S., Moresi, L.N., 2000. Scaling of time-dependent stagnant lid convection: application to small-scale convection on Earth and other terrestrial planets. J. Geophys. Res. 105, 21795–21817.
Solomatov, V.S., Stevenson, D.J., 1993. Suspension in convective layers and style of differentiation of a terrestrial magma ocean. J. Geophys. Res. Planets 98, 5375–5390.
Sotin, C., Grasset, O., Mocquet, A., 2007. Mass–radius curve for extrasolar Earth-like planets and ocean planets. Icarus 191, 337–351.
Sotin, C., Labrosse, S., 1999. Three-dimensional thermal convection in an iso-viscous, infinite Prandtl number fluid heated from within and from below: applications to the transfer of heat through planetary mantles. Phys. Earth Planet. Int. 112, 171–190.
Spiegel, D.S., Fortney, J.J., Sotin, C., 2014. Structure of exoplanets. Proc. Nat. Acad. Sci. U.S.A. 111, 12622–12627.
Stevenson, D.J., Spohn, T., Schubert, G., 1983. Magnetism and thermal evolution of the terrestrial planets. Icarus 54, 466–489.
Tackley, P.J., Ammann, M., Brodholt, J.P., Dobson, D.P., Valencia, D., 2013. Mantle dynamics in super-Earths: post-perovskite rheology and self-regulation of viscosity. Icarus 225, 50–61.
Tackley, P.J., Stevenson, D.J., Glatzmaier, G.A., Schubert, G., 1994. Effects of multiple phase transitions in a 3-dimensional spherical model of convection in Earth's mantle. J. Geophys. Res. 99, 15877–15901.
Unterborn, C.T., Johnson, J.A., Panero, W.R., 2015. Thorium abundances in solar twins and analogs: implications for the habitability of extrasolar planetary systems. Astrophys. J. 806, 139–147.
Valencia, D., O'Connell, R.J., Sasselov, D., 2006. Internal structure of massive terrestrial planets. Icarus 181, 545–554.
Van Laerhoven, C., Barnes, R., Greenberg, R., 2014. Tides, planetary companions, and habitability: habitability in the habitable zone of low-mass stars. Mon. Not. R. Astron. Soc. 441, 1888–1898.
Weinstein, S.A., Olson, P., 1990. Planforms in thermal convection with internal heat sources at large Rayleigh and Prandtl numbers. Geophys. Res. Lett. 3, 239–242.
Zeng, L., Jacobsen, S.B., 2016. A Simple Analytical Model for Rocky Planet Interior. 1606.03522.
Zhang, J., Herzberg, C., 1994. Melting experiments on anhydrous peridotite KLB-1 from 5.0 to 22.5 GPa. J. Geophys. Res. Solid Earth 99, 17729–17742.